Flow-Induced Instability on High-Speed Mini Rotors in Laminar Flow

Emre Dikmen[1]
e-mail: edikmen@gmail.com

Peter J. M. van der Hoogt

André de Boer

Faculty of Engineering Technology,
Section of Applied Mechanics,
University of Twente,
P.O. Box 217,
7500 AE Enschede, The Netherlands

Ronald G. K. M. Aarts

Ben Jonker

Faculty of Engineering Technology,
Section of Mechanical Automation,
University of Twente,
P.O. Box 217,
7500 AE Enschede, The Netherlands

In this study, a modeling approach is developed to examine laminar flow effects on the rotordynamic behavior of high-speed mini rotating machinery with a moderate flow confinement. The existing research work mostly focuses on the flow-induced forces in small gap systems, such as bearings and seals, in which the flow is mostly laminar and inertia effects are ignored. In other studies, medium gap systems are analyzed, taking the inertia effects into consideration, but the surrounding flow is considered as turbulent. However, in high speed mini rotating machinery, the large clearances and the high speeds make the inertia effects significant, even in the laminar flow regime. In the current study, the flow-induced forces resulting from the surrounding fluid are analyzed and these models are combined with the structural finite element (FE) models for determining the rotordynamic behavior. The structure is analyzed with finite elements based on Timoshenko beam theory. Flow-induced forces, which include inertia effects, are implemented into the structure as added mass-stiffness-damping at each node in the fluid confinement. The shear stress is modeled with empirical and analytical friction coefficients, and the stability, critical speeds, and vibration response of the rotor is investigated for different friction models. In order to validate the developed modeling approach, experiments were conducted on a specially designed setup at different support properties. By comparing the experiments with the theoretical models, the applicability of the different friction models are examined. It was found that the dynamic behavior is estimated better with empirical friction models compared to using the analytical friction models.
[DOI: 10.1115/1.4023050]

1 Introduction

Recently, there has been much research work on the design and development of mini rotating machinery (diameters around 10 mm). In most cases, there is a casing around the rotor for protection and for good operating conditions. In these applications, multiphysical effects arising from the surrounding fluid and thermal effects become significant for the rotordynamic studies [1–4]. Due to the high rotation speeds, the air in the confinement formed by the casing and rotor plays an important role on the dynamics of the structure. The surrounding flow alters the natural frequencies and results in rotating damping. The rotating/stationary damping ratio determines the stable operation ranges. In this paper, modeling approaches for the laminar flow of air in the casing are proposed and the obtained models are included in an analysis of the rotordynamic system.

Most of the existing research about the flow effects on rotors concerns the bearings and seals. The reduced gap ratio, $\delta = H/r$ (nominal clearance/rotor radius), in these geometries is around 1/1000. For these applications, the inertia effects are ignored and the flow properties are governed by the Reynolds equation. The derivation of the Reynolds equation, the solution procedure, and rotordynamic coefficients are provided in various textbooks [5–7]. However, fluid inertia effects become significant at high rotation speeds and medium gap ratios (1/10 to 1/100). This condition occurs when $\mathrm{Re}^*/\widetilde{K}_z \geq 1$, where $\widetilde{K}_z$ (shear stress factor) is 12 for laminar flow (which happens $\mathrm{Re}_\delta < 2000$) [6] and modified Reynolds number, $\mathrm{Re}^* = \mathrm{Re}_\delta H/r$. Table 1 illustrates the Couette Reynolds number ($\mathrm{Re}_\delta = \rho\Omega r H/\mu$), at which the fluid inertia effects start to be effective for different gap ratios (Ω is the rotation speed, μ is the fluid dynamic viscosity, and ρ is the fluid density).

Some numerical studies are available in the literature for the calculation of the rotordynamic coefficients (added mass, stiffness, and damping terms), including the inertia effects [8–11]. Coupling this approach to a structural model could be cumbersome, because the fluid numerical model should be applied for different geometries and material properties to obtain the fluid forces and, as a result, the rotordynamic coefficients.

In other studies, the momentum and continuity equations are used and linearized fluid forces are obtained analytically as a function of speed, fluid properties, and geometry. Fritz [12] modeled flow with inertia effects by using an extension of a lubrication theory, in which he included fluid inertia and fluid frictional effects for flow in the annulus. Antunes et al. [13] extended this work by including rotor eccentricity and experimentally verified the developed modeling approach for concentric and eccentric configurations [14]. Both studies use semiempirical friction coefficients and a 2D flow assumption in order to derive added mass, damping, and stiffness. However, these studies do not include the laminar flow regime. In the present study, the friction models for laminar flow are investigated and used for the calculation of flow forces given by Fritz [12] and Antunes et al. [13] for a concentric configuration. Then, these forces are implemented into a structural finite element model (FEM) as added mass, stiffness, and damping. Finite element modeling of the rotor is based on Timoshenko beams (including the flexibility of the rotor shaft). Finally, stability experiments are performed and compared with the theoretical results. In this way, different friction models are examined for predicting the rotordynamic behavior of high-speed rotors in the laminar flow regime.

Table 1 Different gap ratios and Couette–Reynolds number for which fluid inertia becomes significant

H/r	Re_δ
1/10	≥120
1/50	≥600
1/100	≥1200

[1]Corresponding author.

Contributed by the Design Engineering Division of ASME for publication in the Journal of Vibrations and Acoustics. Manuscript received May 21, 2010; final manuscript received September 23, 2012; published online February 25, 2013. Assoc. Editor: Yukio Ishida.

2 Structural Model

Most of the previous studies [12,14] used a simple rigid rotor formulation and coupled this with the rotor forces to study the dynamic behavior. However, small-scale rotating machines operate at much higher velocities than the rigid body mode critical speed and generally also beyond the first flexural mode critical speed [1]. Therefore, a structural model, including the flexibility of the shaft, is required for advanced analysis. The finite element method (FEM) is a widely used discretization technique and is commonly used in the rotordynamic analysis, including the rotor flexibility. In this study, a structural model using FEM based on a simple Timoshenko beam formulation [15,16] is developed [1]. The axial and torsional vibrations are not included. The complex coordinate system is used and the vector of nodal displacements of the element is given as (Fig. 1)

$$\mathbf{q} = [u_{x_1} + iu_{y_1}, \phi_{y_1} - i\phi_{x_1}, u_{x_2} + iu_{y_2}, \phi_{y_2} - i\phi_{x_2}]^T$$

With the use of shape functions' consistent stiffness, mass and gyroscopic matrices for a beam element were derived by Genta [15] (see Appendix A). Furthermore, the damping should be taken into account for the dynamic analysis of the rotating systems. The damping can be classified as rotating damping $\mathbf{C}_r$ and nonrotating damping $\mathbf{C}_n$. The former is the damping related with the stationary parts, whereas the latter is related with the rotating components of a machine. The size of these matrices is the same as the stiffness matrix. The damper elements similar to the spring element can be used to model the damping between different nodes. These elements should be added into the related nodes of the damping matrices. All these matrices are assembled, leading to the governing equation of motion for the structure,

$$\mathbf{M}\ddot{\mathbf{q}} + (\mathbf{C} - i\Omega\mathbf{G})\dot{\mathbf{q}} + (\mathbf{K} - i\Omega\mathbf{C}_r)\mathbf{q} = \Omega^2\mathbf{f}_r e^{i\Omega t} + \mathbf{f}_n(t) \tag{1}$$

A MATLAB code is developed, in which the number of elements, material properties, support stiffness, and damping can be set and then the above matrixes are computed. Next, the unbalance response, the Campbell diagram, and the stable operation ranges can be determined for this structural model. The unbalance response at a certain node is calculated, considering an unbalance force vector $\mathbf{f}_r$ and omitting the nonrotating force vector $\mathbf{f}_n(t)$. The complex eigenvalues in the absence of $\mathbf{f}_r$ and $\mathbf{f}_n(t)$ are obtained at different speeds to determine stable operation ranges and the Campbell diagram [1].

3 Flow-Induced Forces and Friction Models

A model for the friction due to the flow around the rotor is needed to calculate the shear stress and flow-induced forces given by Antunes et al. [13] and Fritz [12]. In these studies, the flow is assumed to be incompressible and two-dimensional and the shear stresses are modeled using semiempirical friction coefficients. By using perturbation methods, linearized fluid forces are obtained per unit length by means of mass-stiffness-damping matrices as

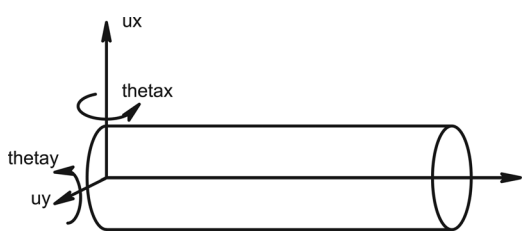

Fig. 1 Beam element

Table 2 Correction factor for three-dimensional flow effects

L/2r	0.1	0.25	0.5	1	2	4	10	∞
c_{3d}	0.01	0.08	0.23	0.51	0.75	0.87	0.95	1

$$\begin{Bmatrix} f_x \\ f_y \end{Bmatrix} = -\begin{bmatrix} m_a & 0 \\ 0 & m_a \end{bmatrix}\begin{Bmatrix} \ddot{u}_x \\ \ddot{u}_y \end{Bmatrix} - \begin{bmatrix} c_1 & c_2 \\ -c_2 & c_1 \end{bmatrix}\begin{Bmatrix} \dot{u}_x \\ \dot{u}_y \end{Bmatrix} - \begin{bmatrix} k_1 & k_2 \\ -k_2 & k_1 \end{bmatrix}\begin{Bmatrix} u_x \\ u_y \end{Bmatrix}$$
$$m_a = \frac{c_{3d}\pi r^2\rho}{\delta}, \quad c_1 = \frac{\Omega m_a c_f}{\delta}, \quad c_2 = \Omega m_a, \quad k_1 = -\frac{\Omega^2 m_a}{4}, \quad k_2 = \frac{\Omega^2 m_a c_f}{2\delta} \tag{2}$$

where c_{3d} is the correction factor for three-dimensional flow effects and given in Table 2 [17].

These flow forces per unit length are multiplied by the element length and lumped into the nodes of each element in the confinement. The assembly procedure is given in more detail in a previous article about multiphysical modeling [1]. The relation between the friction coefficient c_f and the shear stress τ is

$$c_f = \frac{\tau}{\frac{1}{2}\rho v^2} \tag{3}$$

where v is the average flow velocity and taken equal to $\frac{\Omega r}{2}$ in our study. The above formulations are used for friction factors in the turbulent regime [12,13]. Brennen [18] states that this modeling approach could be extended to the laminar regime by using the analytical laminar friction coefficient for idealized two-dimensional flow. The friction coefficient is given by Brennen [18] as

$$c_f = \frac{12\mu}{H\Omega r\rho} \tag{4}$$

Alternatively, there are some studies in the literature where friction is expressed as a function of Reynolds number and geometrical properties using experimental data. Bilgen and Boulos [19] investigated friction coefficients for rotating cylinders having different gap sizes. The results from different studies are fitted into correlations covering different regimes,

$$c_f = 20\frac{\left(\frac{H}{r}\right)^{0.3}}{\mathrm{Re}_\delta} \quad (\mathrm{Re}_\delta < 64) \tag{5}$$

$$c_f = 4\frac{\left(\frac{H}{r}\right)^{0.3}}{\mathrm{Re}_\delta^{0.6}} \quad (64 < \mathrm{Re}_\delta < 500) \tag{6}$$

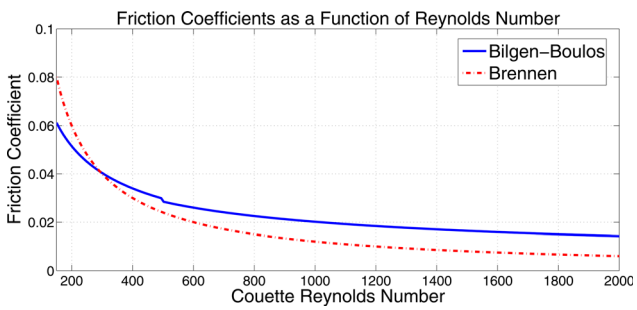

Fig. 2 Models of friction coefficients versus Reynolds number

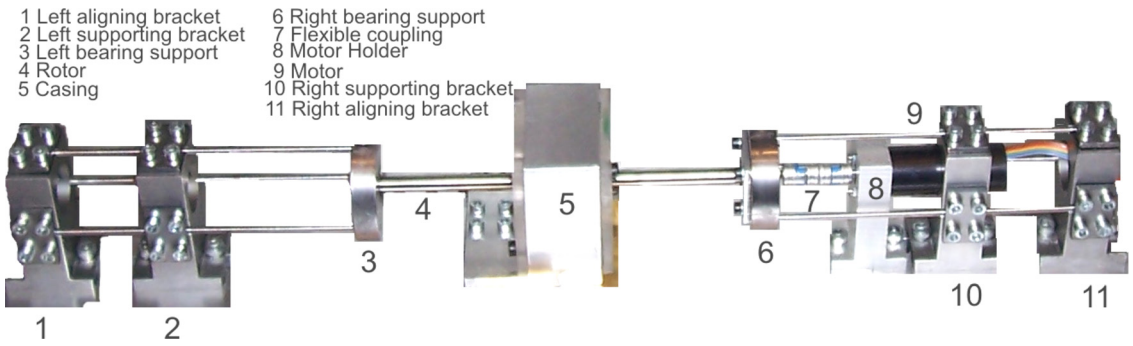

Fig. 3 The complete experimental setup

$$c_f = 2.06\frac{\left(\frac{H}{r}\right)^{0.3}}{\mathrm{Re}_\delta^{0.5}} \quad (500 < \mathrm{Re}_\delta < 10,000) \tag{7}$$

Both friction factors are plotted for a gap ratio (H/r) of 1/50 in Fig. 2 as a function of Couette Reynolds number. For low Couette Reynolds number, the friction coefficients are similar; however, as the Couette Reynolds number increases, the empirical friction coefficient becomes a higher Brennen's value. This can be due to the complex flow effects, which result in considerable differences between the experimentally determined coefficients and the analytical model. This study uses both analytical and experimental friction coefficients to determine the flow forces and evaluated the suitability of each friction modeling approach by comparing the expected stability bounds with experimental data.

4 Experiments

4.1 Setup. Stability experiments were carried out to verify both friction coefficient models. A previously built setup [20] was used (Fig. 3). The experimental setup consists of a stepped rotor (4), casing (5), flexible coupling (7), flexible supports (1, 2, 3, 6, 10, and 11), high speed angular contact ball bearings (3 and 6), and the motor (9). The stiffness and damping of the support structure can be changed by adjusting the length of the support beams. The dimensions and material properties of the setup are described in detail in a previous paper [20].

4.2 Procedure. Firstly, the support properties (stiffness and damping) are determined by modal analysis of the system at standstill for different support beam lengths. A laser Doppler vibrometer (LDV) and an electromechanical shaker are used to measure the vibration of the rotor and the supports. The equivalent stiffness and damping are extracted from these results and implemented into the structural rotor model for theoretical analysis. Finally, spectrum measurements were carried out at different support beam lengths. Spectrum measurements at different speeds were done and also spectrum maps were plotted in order to determine the onset of instability. For plotting the spectrum maps, rotational speeds are varied in steps of 100 rpm and the velocity of the rotor surface is measured. The unbalance of the shaft is the only excitation source.

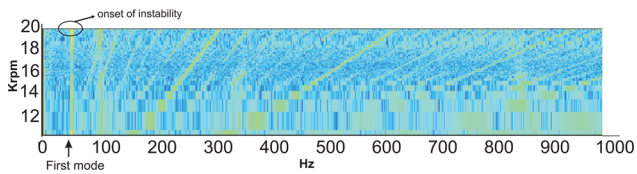

Fig. 4 Spectrum map-support beam length: 80 mm

4.3 Results. The experiments are performed for support beam lengths of 72 mm, 80 mm, and 90 mm. In this way, the effect of the surrounding fluid on the dynamic behavior of the rotor is analyzed for different support stiffnesses.

The surrounding rotating air in the gap between the casing and the rotor gives rise to rotating damping that causes instability. The first mode becomes unstable as the amplitude in the spectrum at that frequency starts to increase drastically. This is revealed experimentally by the spectrum maps. The spectrum map for an 80-mm support beam length is shown in Fig. 4. The amplitude of spectrum related with the first mode starts to increase around 18,000 rpm, and the system becomes unstable.

The numerical calculation of the onset of instability is done by observing the change of decay rate as a function of rotation speed. The decay rate is the imaginary part of the complex frequency, which is the solution of the eigenvalue problem of the equation of motion of the rotor. As the decay rate becomes negative, self-excitation occurs and the system becomes unstable. The numerical prediction of the onset of instability is shown in Fig. 5 for both

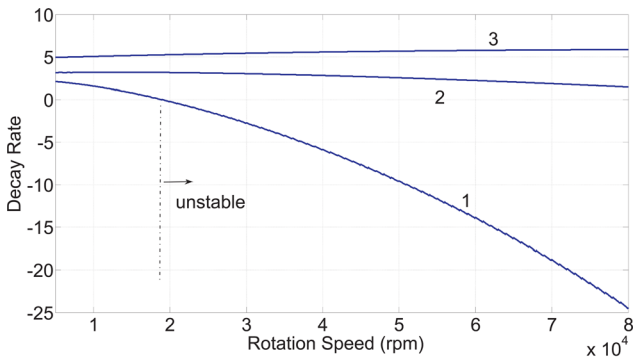

a) Empirical Friction Model (Bilgen-Boulos)

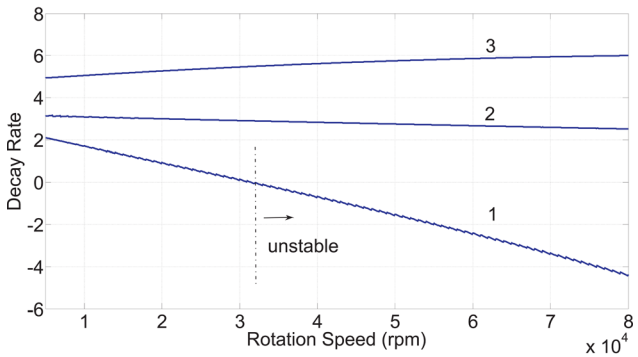

b) Analytical Friction Model (Brennen)

Fig. 5 Onset of instability with different friction models-support beam length: 80 mm

Table 3 Damping and onset of instability in the laminar regime

Support beam length	Damping (Ns/m)	Experiments	Empirical friction model	Analytical friction model
72 mm	2.1	23,840 rpm	21,900 rpm	stable
80 mm	1.86	17,890 rpm	18,900 rpm	stable
90 mm	1.80	15,135 rpm	16,800 rpm	stable

friction models. The decay rates of the first three modes are plotted as a function of rotation speed. The decay rate regarding the first mode becomes negative, and the onset of instability is found out. For the current setup, the flow becomes turbulent at 24,200 rpm. The model which uses the friction coefficient by Brennen predicts stable operation in laminar flow. On the other hand, the empirical friction model estimates instability in the laminar regime. During the experiments, the onset of instability is observed to occur in laminar flow. The onset of instability depends on the ratio between stationary and rotating damping. Table 3 illustrates the stationary damping ratios for different beam lengths and experimental and numerical onset of instability for both friction models.

A reasonable agreement between the theoretical and experimental results is obtained for the empirical friction models given by Bilgen and Boulos [19]. However, the analytical friction coefficients given by Brennen fail to predict the onset of instability in the laminar regime. The observed onset of instability is at relatively high Reynolds numbers, but still in the laminar regime. In the discussion of Fig. 2, it was already noticed that, in this regime, the analytical and the empirical friction coefficients differ considerably. The flow is quite complex (vortices) and the empirically determined friction coefficient model must be used to estimate the unstable operation of the rotor.

5 Conclusions

The stability problems on rotor dynamics of high speed shafts with moderate air gap are outlined. A modeling approach is proposed for flow-induced effects in laminar flow with effective inertia. This approach extends the existing turbulent models by using friction coefficients for shear stress in the laminar flow regime. Two different friction coefficient models are used to calculate the flow-induced forces. The experiments are carried out for different support stiffnesses in order to determine the onset of instability in laminar flow. The numerical and experimental results are compared, and the applicability of the different friction models to estimate the onset of instability is discussed. The use of empirical friction coefficients results in reasonable estimates of dynamic behavior of rotors, with medium gap confinements having high Couette–Reynolds numbers in laminar flow.

Acknowledgment

The support of MicroNed for this research work is gratefully acknowledged. The authors also would like to thank to Jaap Bulsink for his collaboration throughout the design of the experimental setup.

Nomenclature

A = area of the cross-section (m^2)
C = damping matrix (N s/m)
C_r = rotating damping matrix (N s/m)
c_i = damping of the fluid in the gap per unit length (N s/$(m)^2$)
c_f = friction coefficient
E = Young's modulus (Pa)
f_n = nonrotating force vector (N)
f_x = flow-induced forces in x direction per unit length (N/m)
f_y = flow-induced forces in y direction per unit length (N/m)
f_r = force vector resulting from unbalance (N)
G = shear modulus (Pa)
G = gyroscopic matrix (kg), (kg m^2)
H = nominal clearance (m)
I_y = area moment of inertia (m^4)
K = stiffness matrix (N/m), (N/rad)
k = stiffness of the fluid in the gap per unit length (N/m^2)
$\widetilde{K}_z$ = shear stress factor
l = element length (m)
L = rotor length (m)
M = mass matrix (kg), (kg m^2)
M_t = mass matrix related with translational inertia (kg), (kg m^2)
M_r = mass matrix related with rotational inertia (kg), (kg m^2)
m_a = added mass per unit length (kg/m)
q = vector of nodal displacements (m), (rad)
r = rotor radius (m)
Re^* = modified Reynolds number
Re_δ = Couette Reynolds number
u_{x_i} = displacement of ith node in x direction (m)
u_{y_i} = displacement of ith node in y direction (m)
v = gap-averaged tangential velocity (m/s)
δ = reduced gap thickness
μ = dynamic viscosity (Pa s)
Φ = nondimensional variable
ϕ_{x_i} = rotation of ith node in x direction (rad)
ϕ_{y_i} = rotation of ith node in y direction (rad)
ρ = fluid density (kg/m^3)
τ = shear stress (Pa)
χ = shear factor
Ω = rotation speed (rad/s)

Appendix A: Element Matrices for Structural Model

According to Genta [15], the consistent stiffness and gyroscopic matrices for a beam element, Fig. 1, are derived from

$$\boldsymbol{K} = \frac{EI_y}{l^3(1+\Phi)}\begin{bmatrix} 12 & 6l & -12 & 6l \\ & (4+\Phi)l^2 & -6l & (2-\Phi)l^2 \\ & & 12 & -6l \\ & symm. & & (4+\Phi)l^2 \end{bmatrix}$$

$$\boldsymbol{M_T} = \frac{\rho Al}{420(1+\Phi)^2}\begin{bmatrix} m_1 & lm_2 & m_3 & -lm_4 \\ & l^2m_5 & lm_4 & -l^2m_6 \\ & & m_1 & -lm_2 \\ & symm. & & l^2m_5 \end{bmatrix}$$

$$\boldsymbol{M_R} = \frac{\rho I_y}{30l(1+\Phi)^2}\begin{bmatrix} m_7 & lm_8 & -m_7 & lm_8 \\ & l^2m_9 & -lm_8 & -l^2m_{10} \\ & & m_7 & -lm_8 \\ & symm. & & l^2m_9 \end{bmatrix}$$

where $\Phi = \frac{12EI_y\chi}{GAl^2}$ and $m_1 \ldots m_{10}$ are

$$m_1 = 156 + 294\Phi + 140\Phi^2, \quad m_2 = 22 + 38.5\Phi + 17.5\Phi^2,$$
$$m_3 = 54 + 126\Phi + 70\Phi^2, \quad m_4 = 13 + 31.5\Phi + 17.5\Phi^2,$$
$$m_5 = 4 + 7\Phi + 3.5\Phi^2, \quad m_6 = 3 + 7\Phi + 3.5\Phi^2,$$
$$m_7 = 36, \quad m_8 = 3 - 15\Phi,$$
$$m_9 = 4 + 5\Phi + 10\Phi^2, \quad m_{10} = 1 + 5\Phi - 5\Phi^2$$

The consistent mass and gyroscopic matrices are

$$\boldsymbol{M} = \boldsymbol{M_T} + \boldsymbol{M_R}, \quad \boldsymbol{G} = 2\boldsymbol{M_R}$$

References

[1] Dikmen, E., van der Hoogt, P., de Boer, A., and Aarts, R., 2010, "Influence of Multiphysical Effects on the Dynamics of High Speed Mini Rotors, Part I: Theory," ASME J. Vibr. Acoust., **132**, p. 031010.

[2] Epstein, A., 2004, "Millimeter-Scale, Micro Electro-Mechanical Systems Gas Turbine Engines," ASME J. Eng. Gas Turbines Power, **126**, pp. 205–226.
[3] Lin, R. M., and Wang, W. J., 2006, "Structural Dynamics of Microsystems—Current State of Research and Future Directions," Mech. Syst. Signal Process., **20**, pp. 1015–1043.
[4] Meng, G., Zhang, W. M., Huang, H., Li, H. G., and Chen, D., 2009, "Micro-Rotor Dynamics for Micro-Electro-Mechanical Systems (MEMS)," Chaos, Solitons Fractals, **40**, pp. 538–562.
[5] Muszynska, A., 2005, *Rotordynamics*, Taylor and Francis, London.
[6] San Andrés, L., 2008, *Modern Lubrication Theory-Lecture Notes*, Texas A&M University, College Station, TX.
[7] Childs, D., 1993, *Turbomachinery Rotordynamics: Phenomena, Modeling, and Analysis*, Wiley, New York.
[8] Athavale, M., and Przekwas, A., 1994, "A CFD Code for Analysis of Fluid Dynamic Forces in Seals," NASA. Workshop on Seals and Flow Code Development-1993, NASA CP-10136.
[9] Hendricks, R. C., Przekwas, A., Tam, L. T., Muszynska, A., Braun, M. J., and Mullen, R. J., 1988, "Numerical Modeling of Multidimensional Flow in Seals and Bearings Used in Rotating Machinery," National Aeronautics and Space Administration, Lewis Research Center, Technical Report No. TM-100779.
[10] Staubli, T., and Bissig, M., 2001, "Numerically Calculated Rotor Dynamic Coefficients of a Pump Rotor Side Space," International Symposium on Stability Control of Rotating Machinery (ISCORMA), South Lake Tahoe, CA, August 20–24.
[11] Athavale, M., Hendricks, R. C., and Steinetz, B. M., 1995, "Numerical Simulation of Flow in a Whirling Annular Seal and Comparison With Experiments," National Aeronautics and Space Administration, Lewis Research Center, Technical Report No. TM-106961.
[12] Fritz, R. J., 1970, "The Effects of an Annular Fluid on the Vibrations of a Long Rotor, Part 1—Theory," ASME J. Basic Eng., **92**, pp. 923–929.
[13] Antunes, J., Axisa, F., and Grunenwald, T., 1996, "Dynamics of Rotors Immersed in Eccentric Annular Flow. Part I: Theory," J. Fluids Struct., **10**, pp. 893–918.
[14] Grunenwald, T., Axisa, F., Bennett, G., and Antunes, J., 1996, "Dynamics of Rotors Immersed in Eccentric Annular Flow. Part II: Experiments," J. Fluids Struct., **10**, pp. 919–944.
[15] Genta, G., 2005, *Dynamics of Rotating Systems*, Springer, New York.
[16] Genta, G., 1985, "Consistent Matrices in Rotor Dynamics," Meccanica, **20**, pp. 235–248.
[17] Grunenwald, T., 1994, "Comportement Vibratoires d'arbres de Machines Tournantes dans un Espace Annulaire de Fluide de Confinement de Modéré," Ph.D. thesis, Paris University, Paris.
[18] Brennen, C., 1994, *Hydrodynamics of Pumps*, Concepts ETI, Norwich, VT.
[19] Bilgen, E., and Boulos, R., 1973, "Functional Dependence of Torque Coefficient of Coaxial Cylinders on Gap Width and Reynolds Numbers," ASME J. Fluids Eng., **95**(1), pp. 122–126.
[20] Dikmen, E., van der Hoogt, P., de Boer, A., and Aarts, R., 2010, "Influence of Multiphysical Effects on the Dynamics of High Speed Mini Rotors—Part II: Results," ASME J. Vibr. Acoust., **132**, p. 031011.